Borderline Microporous-Ultramicroporous Palladium(II) Coordination Polymers. Effect of Pore Functionalisation on Gas Adsorption Properties.

Jorge A. R. Navarro,*[a] Elisa Barea,[a] Juan M. Salas,[a] Norberto Masciocchi,[b] Simona Galli,[b] Angelo Sironi,[c] Conchi O. Ania[d] and José B. Parra[d]

[a]*Departamento de Química Inorgánica, Universidad de Granada, Av. Fuentenueva S/N, 18071 Granada, Spain, E-mail: jarn@ugr.es (J.A.R. Navarro) Fax: (+34)958248526*

[b]*Dipartimento di Scienze Chimiche e Ambientali, Università dell'Insubria, Via Valleggio 11, 22100 Como, Italy*

[c]*Dipartimento di Chimica Strutturale e Stereochimica Inorganica, Università di Milano and ISTM-CNR, Via Venezian 21, 20133 Milano, Italy*

[d]*Departmento de Energía y Medio Ambiente. Instituto Nacional del Carbón. CSIC Apartado 73, 33080 Oviedo, Spain*

RECEIVED DATE (automatically inserted by publisher);

Keywords: Porous coordination polymers, Hydrogen storage, Crystal structure, X-ray powder diffraction, thermodiffractometry, sodalite, solid-gas adsorption, molecular sieving.

Jorge Andrés Rodríguez Navarro was born in 1969. He obtained his PhD from Granada University in 1996 under the supervision of Prof. J. M. Salas and Prof. M. A. Romero and after a postdoctoral stage at the University of Dortmund, Germany (1997-1999) with Prof. B. Lippert become Associate Professor of Inorganic Chemistry at the University of Granada in 2002. He has co-authored more than 40 papers in peer-reviewed international journals and 1 patent. His research interests are centred on the properties of molecular receptors based on polynuclear coordination compounds. He is particularly interested in the solid-gas and solid-liquid adsorptive properties of flexible porous coordination polymers.

Graphical Contents Entry

An appropriate functionalization of the pyrimidine moiety in the [Pd(μ-X-pymo-N^1,N^3)$_2$]$_n$ polymers (X-Hpymo = 5-X-2-hydroxypyrimidine, X = H, F, Br, I) has a strong effect on their adsorptive properties. In particular, the H and F compounds possess high H_2 adsorption capacities with storage densities of about 0.018 kg H_2/L (77 K) and large isosteric adsorption heats (8-9 kJ/mol).

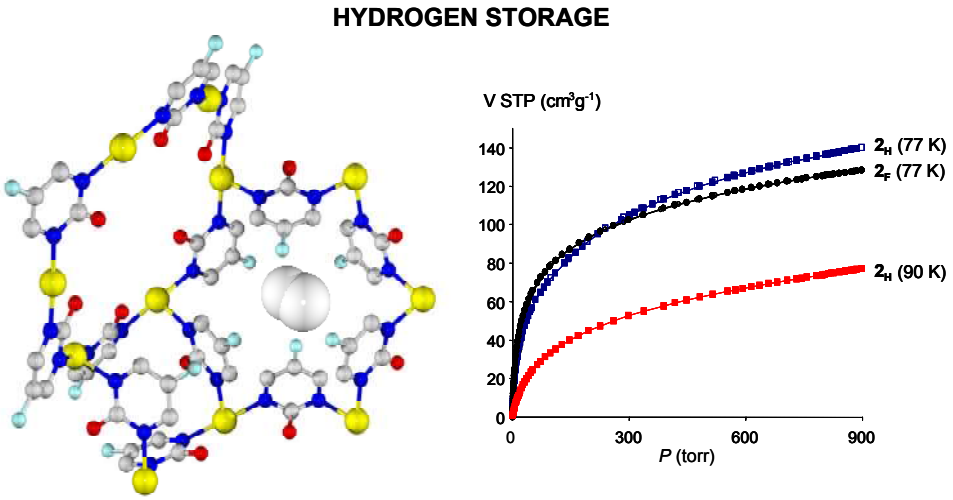

Abstract

Pd^{II} coordination polymers of the $[Pd(\mu\text{-X-pymo-}N^1,N^3)_2\cdot(H_2O)_m]_n$ (X = H, $\mathbf{2_H}$; F, $\mathbf{2_F}$; Br, $\mathbf{2_{Br}}$; I, $\mathbf{2_I}$) type, containing the X-pymo (X-Hpymo = 5-X-2-hydroxypyrimidine) ligands, have been obtained by refluxing aqueous suspensions of the monomeric *trans*-$[Pd(X\text{-Hpymo-}N^1)_2Cl_2]$ ($\mathbf{1_H}$-$\mathbf{1_I}$) precursors with NaOH in a 1:1 ratio. While $\mathbf{2_{Br}}$ and $\mathbf{2_I}$ have been recovered as amorphous materials, the microcrystalline species $\mathbf{2_H}$ and $\mathbf{2_F}$, in their hydrated and anhydrous forms, have been structurally characterized by *ab initio* XRPD methods: square planar Pd^{II} ions, symmetrically connected by exobidentate N^1,N^3 X-pymo bridges, give rise to neutral sodalite zeotypic frameworks (with H_2O guest molecules eventually included in the pores). The thermal properties and porosity have been determined for all the $\mathbf{2_X}$ systems. The H_2, N_2 and CO_2 adsorption isotherms showed that the 2_H and 2_F materials possess permanent porosity, as opposed to $\mathbf{2_{Br}}$ and $\mathbf{2_I}$. Moreover, the isomorphic incorporation of fluorine in the framework causes important modifications in the gas adsorption isotherms; stronger interactions at very low pressures appear (Henry's law region) in all the probes studied (N_2, CO_2 and H_2). Compounds $\mathbf{2_H}$ and $\mathbf{2_F}$ possess high H_2 adsorption capacities at 77 K with respective values of 1.3 and 1.15 weight percentage and storage densities of about 0.018 kg H_2/L, which are combined with large isosteric adsorption heats (8-9 kJ/mol).

Introduction

The high research interest on crystalline microporous materials is boosted by the industrial and environmental applications of molecular separation, gas storage and selective heterogeneous catalysis.[1,2] Porous coordination polymers (PCPs) have recently emerged as a new class of porous materials with improved properties compared to classical ones, *e.g.* zeolites, carbons and oxides, such as lack of non-accessible bulk volume, framework flexibility, and designable micropores.[3] These features have attracted a great deal of attention of many researchers in both the academia[4] and the industry,[5] with about one thousand publications per year on 'coordination polymers', as well as many filed patents.[6]

PCPs with permanent porosity generally have micropores in the 0.5–2 nm range, behaving as adsorbents and heterogeneous catalysts. Ultramicropores, with a pore size less than 0.5 nm have also been achieved in some cases,[7] giving rise to a series of singular features such as entrance blocking effects, molecular sieving properties and unusually high interaction energies with the ultramicropore walls. These characteristics may lead to special orderings of the confined molecules[7] and, eventually, to unusually specific behaviour as reaction vessels.[8]

One of the most outstanding promising uses of PCPs is related to their potential as hydrogen storage materials for mobile applications.[9] Although, relatively large (and optimistic) capacities for hydrogen storage have been reported in the literature,[9] however, most PCPs are characterised by relatively low H_2 heats of adsorption. The latter energy usually lies in the 4.7-7.5 kJ/mol range,[10] rather lower than the estimated 15 kJ/mol value required for reversible H_2 uptake at 298 K and fuel-cell operating pressures between 1.5 and 30 atm.[11] Consequently, it is of high interest the search for alternative PCPs that may exhibit higher enthalpies of adsorption, with minimum penalty in important features such as thermal and mechanical stability.[10,12]

We are currently studying porous metal pyrimidinolates which combine, among other features, permanent porosity with high thermal stability and framework versatility.[13] In this regard, we have very recently communicated the preparation of the thermally robust $[Pd(pymo)_2]_n$ (Hpymo= 2-hydroxypyrimidine) framework (**2$_H$**), which represents, to our knowledge, the first Pd^{II} based PCP and possesses the unusually high H_2 storage density of 0.018 kg H_2/L at 77 K and 900 torr.[14] In the present work, we have extended the study to a series of similar PCPs (**2$_X$**) based on palladium(II) metal ions and 5-X-pyrimidin-2-olate derivatives (X = F, Br, I) with the aim of finely tuning their

structural features and, consequently, their solid-gas adsorption properties. An analogous approach has been already, successfully employed with the isostructural series of $[M(X\text{-pyrimidin-2-olate})_2]_n$ (M = Co, Zn; X = H, Cl, Br, I) diamondoid coordination polymers, whose structural, thermal and magnetic properties have been modulated by changing the X substituent on the pyrimidinic ring.[15]

Results and Discussion

Synthesis

The base-promoted polymerisation of a suspension of the $[Pd(X\text{-Hpymo})_2Cl_2]$ materials ($\mathbf{1_X}$, X = H, F, Br, I; X-Hpymo = 5-X-2-hydroxypyrimidine) leads to the self assembly of 3D microporous sodalitic networks of the $[Pd(X\text{-pymo})_2(H_2O)_m]_n$ type ($\mathbf{2_X}$) (Scheme 1). Although simple, this process, involving Pd^{II} ions, has been reported by us for the first time.[14] In this regard, the formation of PCPs usually implies a self-assembly process of metal fragments and organic spacers, which is facilitated by the use of labile metal ions (*i.e.* first row, divalent transition metal ions; Cu^{I}, Ag^{I}, Zn^{II} and Cd^{II}).[3] Pd^{II} possesses an intermediate robustness, which makes it adequate for obtaining stable, discrete polynuclear systems, with cavities and voids ready for molecular recognition and catalytic processes.[16] However, to the best of our knowledge, before our studies, this metal ion has not yet been employed for the construction of crystalline porous coordination polymers. Moreover, the less labile nature of the Pd^{II} ions hampers the crystallisation of the PCPs in the form of single crystals, and leads mainly to the formation of microcrystalline or amorphous solids. As demonstrated below, these polycrystalline materials can be structurally characterised by X-ray powder diffraction (XRPD), using ab-initio techniques[17] and thermodiffractometric measurements.

Crystal structures of the hydrated and anhydrous forms of $\mathbf{2_F}$

Both the hydrated and the anhydrous forms of $\mathbf{2_F}$ crystallise in the cubic space group *Pn-3m*, the asymmetric unit consisting of one metal ion, in *2.mm* (*f* Wyckoff position), and one F-pymo ligand lying about a crystallographic mirror plane bisecting the oxygen and fluorine atoms (*k* Wyckoff position). In the case of the hydrated form, two water molecules, lying about a crystallographic mirror plane (*k* Wyckoff position), further complete the asymmetric unit.

The two crystal structures are characterized by square planar Pd^{II} ions, *ca.* 5.7 Å apart, connected through N^1,N^3-exobidentate F-pymo bridges (Figure 1a). The presence of the ligands' bridging defines three different structural motives, namely, planar molecular hexagons, metallacalix[4]arenes and metallacalix[6]arenes (Figure 1b), which interlock each other to build a 3D open framework of the sodalite zeotype (Figure 1c).

In the hydrated $[Pd(F\text{-}pymo)_2(H_2O)_2]_n$ parent, no bonding interaction is at work between the metal centres and the oxygen atoms of the water molecules: indeed, the shortest Pd···O contact is 4.81 Å. The same characteristic was already found in $[Pd(H\text{-}pymo)_2(H_2O)_2]_n$, where the shortest Pd···O contacts were above 5.0 Å.[14c] Moreover, the fluorine atoms are not involved in non-bonding interactions but, in the hydrated form, were water molecules cluster around the hexagonal windows at distances, from its centre, of 1.59 or 3.22 Å and form weak hydrogen bonds with the exocyclic oxygen atoms of the F-pymo ligands (~ 2.97 Å).

Dehydration of the $[Pd(F\text{-}pymo)_2(H_2O)_2]_n$ precursor does not imply a significant unit cell volume modification, the $\mathbf{2_F}$ framework thus being rigid, even slightly more so than that of $\mathbf{2_H}$ (Table 1). At variance, the distorted, *rhombohedral* $[Cu(H\text{-}pymo)_2(H_2O)_m]_n$, on losing its water molecules, does suffer a non negligible V/Z modification.[14c]

The presence of the fluorine substituent on the pyrimidine ring implies a 2.5% loss in the accessible empty volume of anhydrous $\mathbf{2_F}$ with respect to $\mathbf{2_H}$ (Table 1), as well as a 30% shrinkage of the β-cage diameter (5.7 Å *vs.* 8.1 Å).

Thermal behaviour

The thermal performance of the $\mathbf{2_X}$ materials has been studied by thermogravimetry, differential scanning calorimetry and thermal X-ray powder diffraction. These systems easily dehydrate (40-90 ºC), suggesting weak or none interactions between the guest water molecules and the d^8 square planar Pd^{II} centres. At least in the case of $\mathbf{2_H}$ and $\mathbf{2_F}$, this is structurally confirmed by the absence of Pd-O bonds (see previous paragraph). In contrast, in $[Cu(4H\text{-}pymo)_2(H_2O)_m]_n$ (4H-pymo = pyrimidine-4-olate), where significant apical Cu-O bonds [2.76(3) Å] at the Cu^{II} ions are present, dehydration occurs at a slightly higher temperature (up to 160 °C).[14b]

In addition, the $\mathbf{2_X}$ series possesses a remarkable high thermal stability in a reactive atmosphere of air; indeed, their decomposition temperatures, as high as 370 °C, follow the trend 315 ºC ($\mathbf{2_I}$), 325 ºC ($\mathbf{2_{Br}}$), 330 ºC ($\mathbf{2_H}$), 370 ºC ($\mathbf{2_F}$).

We have also monitored, by XRPD, the dehydration processes of crystalline $\mathbf{2_H}$ and $\mathbf{2_F}$, determining the lattice parameter changes during heating. The results, shown in Figure 2a for both compounds, share the same qualitative trend in both cases: a slight cell volume decrease at lower temperatures, attributed to the loss of the guest water molecules, is followed by an increase, due to thermal expansion. As anticipated above, Figure 2a also indicates that $\mathbf{2_F}$ is slightly more rigid than $\mathbf{2_H}$. For both $\mathbf{2_H}$ and $\mathbf{2_F}$, dehydration occurs smoothly without the formation of intermediate (amorphous or crystalline) phases. The dehydration process is fully reversible for both materials, as substantiated by the data reported in Figure 2b for $\mathbf{2_H}$, where the lattice parameters measured during heating are perfectly matched by those observed on cooling, *including the water sorption effect below 45 °C.*

Finally, taking into account the *relative* small changes in the lattice parameters, it is clear that these porous frameworks do not undergo significant stress during heating, since a $\partial \ln V/\partial T$ value of only 5.3 10^{-6} K^{-1} can be computed (for $\mathbf{2_F}$), falling well below that of other materials of this kind, more than ten times higher.[18]

Gas sorption properties

The gas adsorption properties of the anhydrous $\mathbf{2_X}$ solids towards N_2, CO_2 and H_2 have been studied in order to determine their textural properties and their potential use for gas separation and storage purposes.

Figure 3 shows the adsorption isotherms of N_2 at 77 K for the $\mathbf{2_H}$ and $\mathbf{2_F}$ PCPs. $\mathbf{2_H}$ displays a type I-IV hybrid shape isotherm, with a hysteresis loop (type H1) at relative pressures above 0.8, with is attributed to textural mesoporosity arising from interparticle (voids) mesopores. The isotherm also exhibits a sharp knee at low relative pressures ($p/po \sim 0.01$), followed by a *plateau* (corresponding to the filling of the monolayer), indicating that the permanent porosity of the sample is mainly composed of micropores, of rather uniform size. The $\mathbf{2_F}$ sample shows a typical type I isotherm, with a steep rise at low relative pressures, confirming the presence of micropores and the absence of mesoporosity from interparticle condensation. Moreover, a pronounced difference is observed: the isotherm of $\mathbf{2_F}$ is characterized by an upward step located in the range $0.01 < p/po < 0.05$, along with a hysteresis cycle in the desorption branch at the same relative pressures range. Similar stepwise and hysteretic gas adsorption has been previously reported in certain highly crystalline samples such as zeolites and carbons obtained via template methods[19], and porous metal organic frameworks. [20,21]

The origin of this unusual behaviour has not yet been clarified and various hypotheses have been proposed. Some authors suggest that it might be linked to blocking effects[22] -that in our case would be exerted by the fluorine residues of the β-cage hexagonal windows defined by the metallacalix[6]arene (Figure 1), to "breathing" or "swelling" effects in the flexible framework of the PCP,[3,4] or linked to a phase transition in the nitrogen adsorbate.[20] The position of the low-pressure hysteresis loop has also been related to the presence of defects in the crystals[19].

The nitrogen adsorption data displayed in logarithmic scale in Figure 3, shows that both isotherms are somewhat parallel at low relative pressures (Henry's law region), being the uptake higher in $\mathbf{2_F}$. On the other hand, the isotherms practically superimpose at p/po> 0.05, after filling of the monolayer; this behaviour suggests stronger interactions between the adsorbate and the framework in the $\mathbf{2_F}$ counterpart. Fluorine functionalisation does not have an effect on the BET surface area with a value of 600 m^2g^{-1} for both materials, since the isotherms practically overlay in the range of application of the BET model (0.05-0.35).

Since neither slow diffusion was observed during equilibration nor was adsorption shifted to higher pressures on passing from $\mathbf{2_H}$ to $\mathbf{2_F}$. Thus, the results point out that there seems not to be any diffusional constriction hindering the accessibility of N_2 to the micropores. In other words, it seems that the samples present similar microporous structure (as seen by nitrogen), with the adsorbate strongly adsorbed in the $\mathbf{2_F}$ sample. Taking also in account the framework rigidity of $\mathbf{2_F}$, the most plausible explanation for the upward step at low relative pressures would be linked to a phase transition in the nitrogen adsorbate, as reported in the literature for ultramicroporous materials.[19,20] Nevertheless, further research on adsorption of several gases at different temperatures and pressures is currently ongoing to clarify this issue and to confirm this premise.

A bulk effect of the pyrimidine ring substituents (assuming *local* structural identity) is confirmed by the behaviour of $\mathbf{2_{Br}}$ and $\mathbf{2_I}$ with a lack of N_2 adsorption, suggesting negligible porosity accessible to nitrogen probe in both samples. Indeed, due to the nearly uncompressible nature of this 3D framework and to the size of the Br and I atoms, very short inter-halogen distances would be generated in hypothetic $\mathbf{2_{Br}}$ and $\mathbf{2_I}$ sodalitic networks (2.32 and 2.12 Å, respectively, admitting C-Br and C-I bonding distances of 1.85 and 2.10 Å). This implies that *crystalline* species with Br-pymo and I-

pymo, isomorphous to $\mathbf{2_H}$ and $\mathbf{2_F}$, *cannot* be formed. The shortest allowed inter-halogen distance, indeed, appears that present in the anhydrous $\mathbf{2_F}$, *i.e.* F···F = 2.84 Å. Apparently, *but for completely different reasons*, Cl, Br and I substitution (but not F!) are well tolerated in the isomorphous $[M(X\text{-pymo})_2]_n$ (M = Co and Zn) diamondoid frameworks, for which *attractive* intermolecular forces (of the =O···X kind[23]) for the heaviest halogens are at work.[15]

The CO_2 adsorption measurements indicate that the whole $\mathbf{2_X}$ series possesses permanent porosity in the microporous-ultramicroporous region, which is in good agreement with the shapes of the nitrogen adsorption data (see Figure 4). The amount of CO_2 adsorbed at 293 K and 650 torr follows the trend 10 cm^3g^{-1} ($\mathbf{2_I}$), 18 cm^3g^{-1} ($\mathbf{2_{Br}}$), 40 cm^3g^{-1} ($\mathbf{2_H}$) and 61 cm^3g^{-1} ($\mathbf{2_F}$)**.** The high CO_2 storage capacity of $\mathbf{2_H}$ and $\mathbf{2_F}$ at room temperature should be indicative of the full accessibility of the adsorbate molecules to their porous network. The higher performance of $\mathbf{2_F}$ compared to $\mathbf{2_H}$ is probably related to the presence of specific Lewis acid-base interactions, of the F···CO_2 type. Similar evidences for large chemical selectivity in gas sorption properties have indeed been recently communicated for Cr-based MOF's containing "inorganic" F atoms[24] or, *even if reversed*, for OH···CO_2 interactions.[25] The lower performance of $\mathbf{2_I}$ and $\mathbf{2_{Br}}$ materials is in good agreement with their amorphous nature, indicating that a 3D and porous network is not formed when atoms of large dimensions are incorporated in the pyrimidinic ring. The isosteric heats of CO_2 adsorption for $\mathbf{2_H}$ and $\mathbf{2_F}$ samples where evaluated according to the Clausius-Clapeyron (equation 1) from the adsorption isotherms measured at 273 and 293 K (Figure 4):

$$q_{st} = -R\left(\frac{\delta \ln P}{\delta (1/T)}\right)_N \quad (1)$$

where q_{st}, R, P, and N represent isosteric heat of adsorption, gas constant, pressure, and amount of adsorption of CO_2, respectively. The results show unusually high isosteric adsorption heat values in the range of 38-44 kJ/mol and 40-48 kJ/mol for $\mathbf{2_H}$ and $\mathbf{2_F}$, respectively. These observations agree with a strong adsorbate-adsorbent interaction and are higher than the values for physisorption on mesoporous silicas (*ca.* 20.0 kJ/mol) and on the chromium/aluminium metalorganic framework MIL-53 (35 kJ/mol),[25] and close to the values for aluminosilicate zeolites (50-70 kJ/mol).[26]

These results also confirm those obtained from nitrogen adsorption; assuming that both samples present almost the same porous network, the larger quadrupolar moment of the CO_2 molecule might interact with the F atoms and thereby the adsorption is stronger and the uptake is higher. In the case of nitrogen its quadupolar moment is considerably smaller, although it seems to be also "perturbed" by the fluorine atoms.

Figure 5 shows the H_2 adsorption isotherms corresponding to $\mathbf{2_H}$ and $\mathbf{2_F}$ PCPs at 77 K and 90 K. Since hydrogen is a supercritical gas at these temperatures, its adsorption isotherms are of type 1. Moreover, their fully reversible character indicates that only physisorption in the micropores is occurring and that there is a lack of irreversible interactions with the metallic centers on the framework. It is noteworthy the steeper slope of the $\mathbf{2_F}$ isotherm in the low pressure range, suggesting again stronger interactions compared to $\mathbf{2_H}$. Noteworthy, the two species possess a relevant capacity of H_2 storage at 77 K and 900 torr: *ca.* 1.3% and 1.15% weight percentage, respectively. This results in high storage densities (i.e., volumetric capacities), *ca.* 0.018 kg H_2/L for both materials. The volumetric capacities of $\mathbf{2_H}$ and $\mathbf{2_F}$ overcome the highest values reported so far, observed for PCPs-type materials *at similar experimental conditions;* namely 0.017 kg H_2/L for MOF-505 [Cu_2(bptc)],[27] or a gravimetric capacity of 2.47% at 77 K and 760 torr. Another implication of the gas sorption performances of $\mathbf{2_H}$ and $\mathbf{2_F}$ is the relative surface coverage of H_2 molecules[28] (83%), which is among the highest known values, *i.e.* $Mn(HCOO)_2$[29] (150%), $Cu_3[Co(CN)_6]_2$ (94%),[30] [Cu_2(bptc)] (52%),[27] zeolite HSSZ-13[31] (76%) and highly activated porous carbon materials (38%).[1b]

Although some of the values of hydrogen storage capacity at 77 K for PCPs are high, the relatively low H_2 adsorption heats could be a limitation for room temperature use at safe pressures (see above).[10] In order to evaluate the energy of the H_2-PCP interaction we have calculated the isosteric heats of adsorption for $\mathbf{2_H}$ according to the Clausius-Clapeyron equation 1 by using the H_2 adsorption isotherms measured at 77 and 90 K (Figure 5). The results show high isosteric adsorption heats in the range 8-9 kJ/mol (Figure 6), which are close to the estimated 15 kJ/mol required for reversible H_2 uptake at 298 K and fuel-cell operating pressures between 1.5 and 30 atm.[11] Moreover, the steeper slope of the $\mathbf{2_F}$ isotherm in the low pressure range compared to $\mathbf{2_H}$ should be indicative of an even higher adsorption energy. Another remarkable feature of the $\mathbf{2_H}$ and $\mathbf{2_F}$ materials is the high density of the adsorbed H_2 molecules in the pores, with respective values of 0.047 kg/L and 0.053 kg/L, which approach the 0.0708 kg/L density of liquid hydrogen at 20 K.

Experimental Section

Materials and Physical Measurements

2-Hydroxypyrimidine·HCl, 5-fluoro-2-hydroxypyrimidine, N-bromosuccinimide and N-iodosuccinimide were purchased from Aldrich and K_2PdCl_4 from Johnson-Matthey. 5-bromo-2-hydroxypyrimidine and 5-iodo-2-hydroxypyrimidine[32] and *trans*-$[PdCl_2(X\text{-}Hpymo)_2]$ (**1$_X$**, X = H, F, Br, I)[14] and $[Pd(pymo)_2]_n$ (**2$_H$**)[14] were prepared according to literature methods.

Elemental (C,H,N) analyses were obtained at a Fisons - Carlo Erba EA 1008 analyser. Thermogravimetric and calorimetric analyses were performed in air on a Schimadzu-TGA-50H and on a Shimadzu DSC-50 equipments, respectively (all these instruments are in Centre of Scientific Instrumentation of the University of Granada). IR spectra were recorded on a ThermoNicolet IR 200 spectrophotometer by using KBr pellets. Sorption isotherms were measured in a Micromeritics 2010 M (Instituto Nacional del Carbón, CSIC, Oviedo) and Micromeritics Tristar 3000 (Universidad de Granada) volumetric instruments under continuous adsorption conditions. Prior to measurement, powder samples were heated at 130 °C for 2 h and outgassed to 10^{-3} Torr using a Micromeritics Flowprep. BET analysis has been used to determine the total specific surface area for the N_2 isotherms. The isosteric adsorption heats for H_2 and CO_2 have been determined from the adsorption isotherms at two different temperatures (77 and 90 K for H_2 and 273 and 293 K for CO_2) using the Clausius–Clapeyron equation.

*Synthesis of **2$_F$**, **2$_{Br}$**, **2$_I$**.*

A water suspension of the corresponding **1$_X$** precursor (3 mmol in 50 mL of H_2O) was treated with 30 mL of 1 M NaOH. The resulting pale yellow suspension was refluxed for 20 h affording pale yellow microcrystalline powders for **2$_H$**, **2$_F$** or amorphous yellow powders for **2$_{Br}$**, **2$_I$**. Yields: 98-99%. **2$_F$** Calcd. for $[Pd(C_4H_2N_2OF)_2]\cdot 2H_2O$: C, 26.07; H, 2.19; N, 15.20; found: C, 26.03; H, 1.77; N, 15.16. **2$_{Br}$** Calcd. for $[Pd(C_4H_2N_2OBr)_2]\cdot 1.5H_2O$: C, 19.96; H, 1.47; N, 11.64; found: C, 19.82; H, 1.31; N, 11.64. **2$_I$** Calcd. for $[Pd(C_4H_2N_2OI)_2]_n\cdot 2H_2O$: C, 16.44; H, 1.38; N, 9.58; found: C, 16.40; H, 1.07; N, 9.54.

X-Ray Powder Diffraction Characterisation

Analytical measurements. X-ray powder diffractograms (CuK_α, λ = 1.5418 Å) were acquired on a BRUKER AXS D8 (University of Insubria) or on a PHILIPS PW100 diffractometer (University of Granada). Thermodiffractometry was performed on the θ:θ Bruker AXS D8 diffractometer equipped with an aluminium sample holder located in a remotely-controlled heating stage assembled by Officina Elettrotecnica di Tenno, Italy. Nominal thermal stability: ±0.1 °C. The thermal expansion coefficients have been determined by computing the slope of the (a/a_0-1) and (V/V_0-1) *vs.* T curves.

Ab-initio XRPD structural analysis of $\mathbf{2_F}$. The powders were gently ground in an agate mortar, then cautiously deposited in the hollow of an aluminium holder 0.2 mm deep containing a zero-background quartz plate. Diffraction data (CuK_α, λ = 1.5418 Å) were collected on a θ:θ Bruker AXS D8 diffractometer. In the case of the hydrated species, the diffractometer was equipped with primary and secondary Soller slits (2.3°), divergence, antiscatter and receiving slits (0.5°, 0.5° and 0.2 mm, respectively), secondary beam curved graphite monochromator, Na(Tl)I scintillation detector and pulse height amplifier discrimination. Nominal resolution for the present set-up is 0.07° 2θ (FWHM of the α_1 component) as measured from the Si(111) peak at 28.44° (2θ). In the case of the anhydrous compound, the diffractometer was equipped with primary (2.3°) and secondary (2.5°) Soller slits, divergence and receiving slits (0.5° and 8°, respectively), a linear position sensitive detector and pulse height amplifier discrimination. The generator was operated at 40 kV and 40 mA with both set-ups. Long step-scans, with $\Delta 2\theta = 0.02°$, were performed overnight in the $5 < 2\theta < 105°$ range, at r.t. for the the hydrated form, at 130 °C for the anhydrous one, taking advantage of the heating-stage.

Visual inspection of the acquired diffractograms suggested isomorphism with the $\mathbf{2_H}$ phases, thus prompting us to adopt *Pn-3m* as the probable space group, and *a* = 16.3 Å as the initial cell parameter, subsequently checked with Le Bail refinements with Topas-R.[33] The space group and cell choices were definitely confirmed by successful solutions and refinements. The structure models were base on those derived by using the simulated annealing[34] technique implemented in Topas-R for the pristine $\mathbf{2_H}$ phases. The F-pymo ligand was treated as a rigid body, by applying mean bond distances and angles derived from the literature (C-C, C-N = 1.35 Å, C-H = 0.95 Å, C-O = 1.25 Å, C-F = 1.35 Å). The final refinements were performed by the Rietveld method using

Topas-R. In order to stabilize convergence to a chemically sound model, a soft restraint on the Pd-N bond distance (1.95 Å) was introduced and the description of the organic ligand as a rigid body maintained. Peak shapes were described by the fundamental parameters approach.[35] The experimental background was fit by a polynomial description. Systematic errors were modelled with sample-displacement angular shifts. Metal atoms were given a refinable, isotropic displacement parameter (B_M), while lighter atoms were assigned a common $B = (B_M + 2.0)$ Å^2 value. Scattering factors, corrected for real and imaginary anomalous dispersion terms, were taken from the internal library of Topas-R. Final R_p, R_{wp}, R_{Bragg}, and χ^2 agreement factors, details on data collections and analyses can be found in Table 2. Figure 7 shows the final Rietveld refinement plots.

Crystallographic data (excluding structure factors) for the three reported structures have been deposited with the Cambridge Crystallographic Data Centre as supplementary publications No. CCDC ####. Copies of the data can be obtained free of charge upon application to CCDC, 12 Union Road, Cambridge CB2 1EZ, U.K. (fax, (+44)1223 336-033; e-mail, deposit@ ccdc.cam.ac.uk).

Conclusions

A series of thermally robust PCPs with permanent porosity has been synthesized and the effect of their functionalisation on the adsorptive properties towards certain probes has been evaluated. In particular, bromine and iodine functionalisation was found to disrupt the sodalitic framework, while substitution of the 5-H atom by fluorine has a remarkable effect on both the thermal robustness and adsorptive properties, with a significant enhancement of the adsorption energy of the guest molecules included in the pores. The incorporation of fluorine atoms strongly affects the interaction energies of the probes with the adsorbate, likely as a consequence of the perturbation of their quadrupolar moments by the electronic density of fluorine atoms.

The high H_2 uptake, combined with high adsorption energies, is indicative of an optimal size of the pores and of the presence of highly exposed metal centers in the porous frameworks. This unusual characteristics turns out in extremely high volumetric capacities for hydrogen storage, that is of paramount importance for practical applications.

We have further completed the characterization of the $[Pd(X\text{-}pymo)_2]_n$ PCPs, not only adding experimental observations based on thermodiffractometric measurements,

but also demonstrating, and interpreting, their framework rigidity and stability, which are important technological requirements for the safe and long-lasting usage of devices or storage tanks derived therefrom.

Comparison with the analogous $[M(X\text{-pymo})_2]_n$ diamondoid PCPs, based on tetrahedral, and not square planar, metal geometry, has further shown how the halogen size and nature differently affect the formation of isomorphous series, stabilizing, or unfavouring, the Br and I-pymo derivatives.

Work can be anticipated in the direction of preparing and characterizing, in their peculiar sorption functional properties, new F-pymo derivatives with more flexible ions, like copper(II), or less rigid topological arrangements.

Acknowledgements

The Spanish Ministry of Education and Science (CTQ-2005-00329/BQU, EB Postdoctoral Grant (EX2005-1004)) and Junta de Andalucia are acknowledged for funding. We also thank the Fondazione Provinciale Comasca for partial finantial support.

Table 1. Unit cell and empty volumes for the hydrated and anhydrous $\mathbf{2_H}$ and $\mathbf{2_F}$ materials; BET surface area (calculated from the N_2 isotherm at 77 K), and sorption properties toward CO_2 at 293 K and 650 torr, and H_2 at 77 K and 900 torr (weight % and storage density).

	Cell V ($Å^3$)	Cell V; Empty V ($Å^3$) % Void	BET Area ($m^2\ g^{-1}$)	Ads N_2 77 K, 76 torr ($cm^3\ g^{-1}$)	Ads CO_2 293 K, 650 torr ($cm^3\ g^{-1}$)	Ads H_2 77 K, 900 torr	
	RT hydrated	**130 °C anhydrous**				**Weight %**	**kg H_2 L^{-1}**
$\mathbf{2_H}$	4315	4364; 1801 41.3	600	150	40	1.3	0.018
$\mathbf{2_F}$	4340	4327; 1678 38.8	600	149	61	1.15	0.018

Table 2. Crystallographic data and refinement parameters for the hydrated and anhydrous $\mathbf{2_F}$ materials.

	hydrated $\mathbf{2_F}$	**anhydrous $\mathbf{2_F}$**
Formula	$C_8H_8F_2N_4O_4Pd$	$C_8H_4F_2N_4O_2Pd$
M_r (g mol^{-1})	368.59	332.56
Crystal System	cubic	cubic
Space Group	Pn-3m	Pn-3m
a (Å)	16.3114(8)	16.2957(8)
V (Å^3)	4339.8(7)	4327.3(7)
Z	12	12
T (K)	298(2)	400(2)
λ (Å)	1.5418	1.5418
ρ_{calcd} (g/cm^3)	1.692	1.531
μ (mm^{-1})	10.73	10.59
F(000)	2160	1920
refinement 2θ range (°)	5-105	5-105
Data / Restr / Param	5001 / 1 /11	5001 / 1 / 10
R_p, R_{wp} [a]	0.116, 0.149	0.112, 0.083
R_{Bragg} [b]	0.080	0.080
χ^2 [c]	1.712	5.025

[a] $R_p = \Sigma_i|y_{i,o} - y_{i,c}|/\Sigma_i|y_{i,o}|$, $R_{wp} = [\Sigma_i w_i(y_{i,o} - y_{i,c})^2/\Sigma_i w_i(y_{i,o})^2]^{1/2}$. [b] $R_{Bragg} = \Sigma_n|I_{n,o} - I_{n,c}|/\Sigma_n I_{n,o}$. [c] $\chi^2 = \Sigma_i w_i(y_{i,o} - y_{i,c})^2/(N_{obs} - N_{par})$, with $y_{i,o}$ and $y_{i,c}$ the observed and calculated profile intensities; $I_{n,o}$ and $I_{n,c}$ the observed and calculated Bragg reflections, respectively, and $w_i = 1/y_{i,o}$.

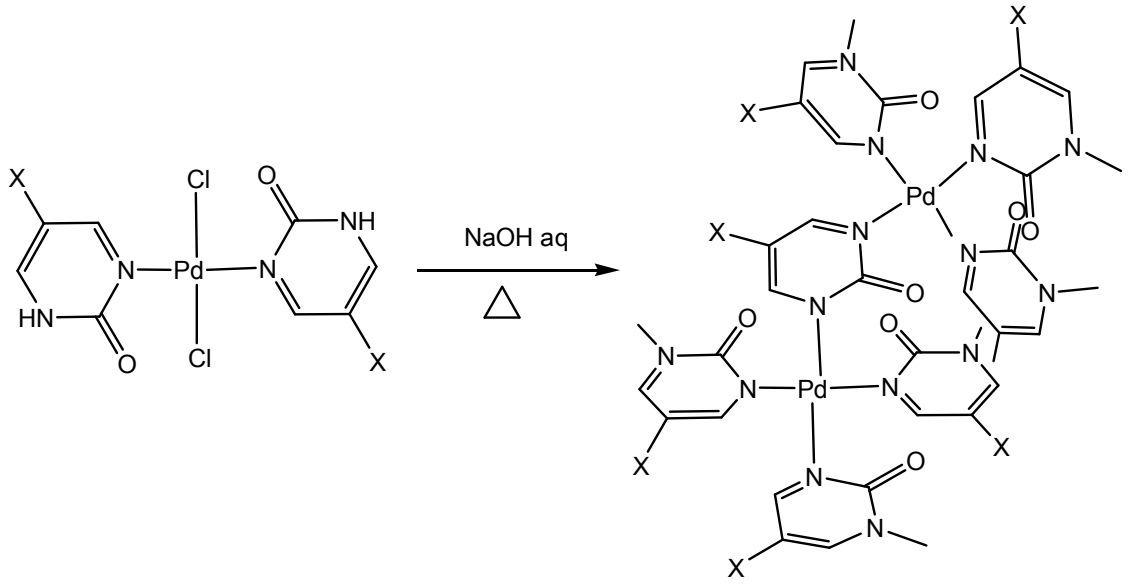

1_X **2_X**

Scheme 1

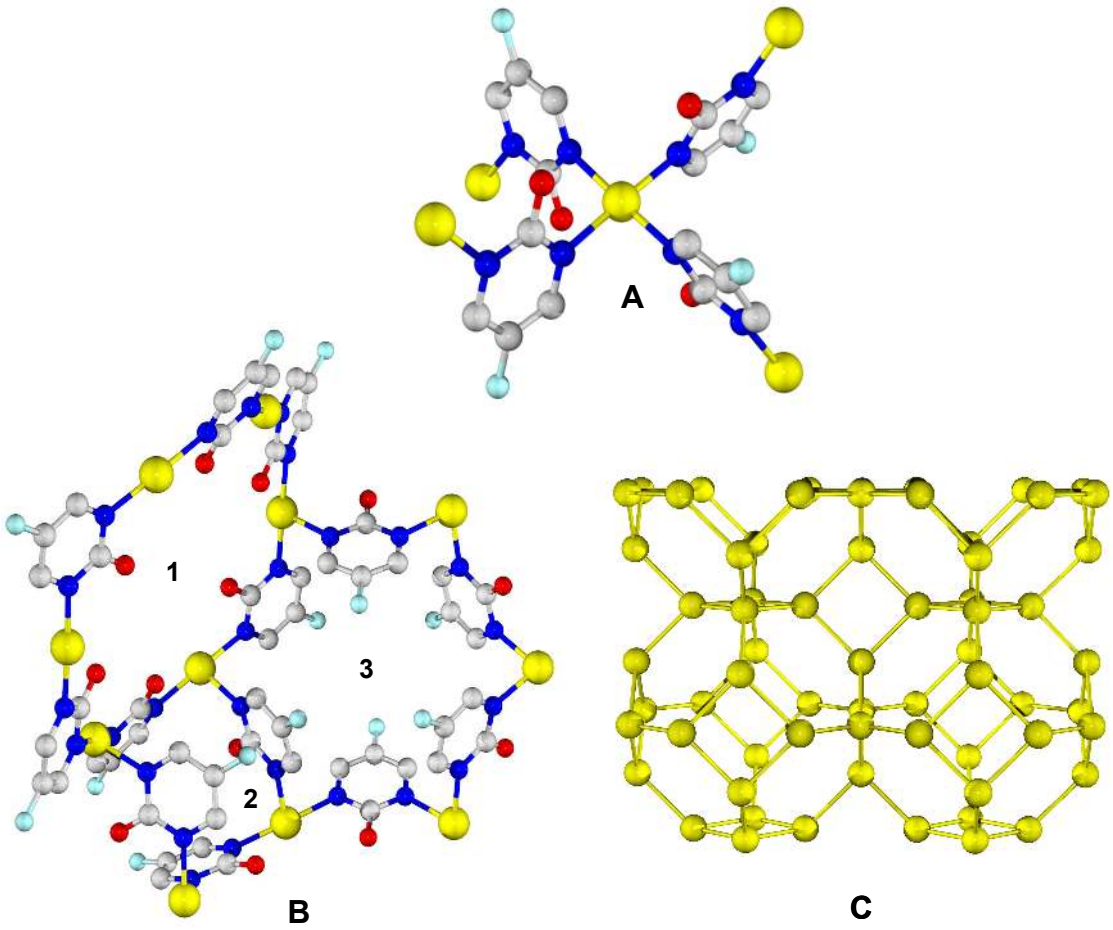

Figure 1. Representation of a) square-planar coordination environment of the Pd centres; b) the three structural motives present in the crystal structures of the hydrated and the anhydrous forms of $\mathbf{2_F}$: 1) planar molecular hexagon, 2) metallacalix[4]arene and 3) metallacalix[6]arene; c) the three dimensional sodalitic framework, where the vertices are the metal centres, the edges represent the bridging ligands. Pd, yellow; C, grey; N, blue; O, red; F, cyano. The hydrogen atoms have been omitted for clarity purposes. The coordinates have been taken from the hydrated form; at the drawing level the two structures appear identical.

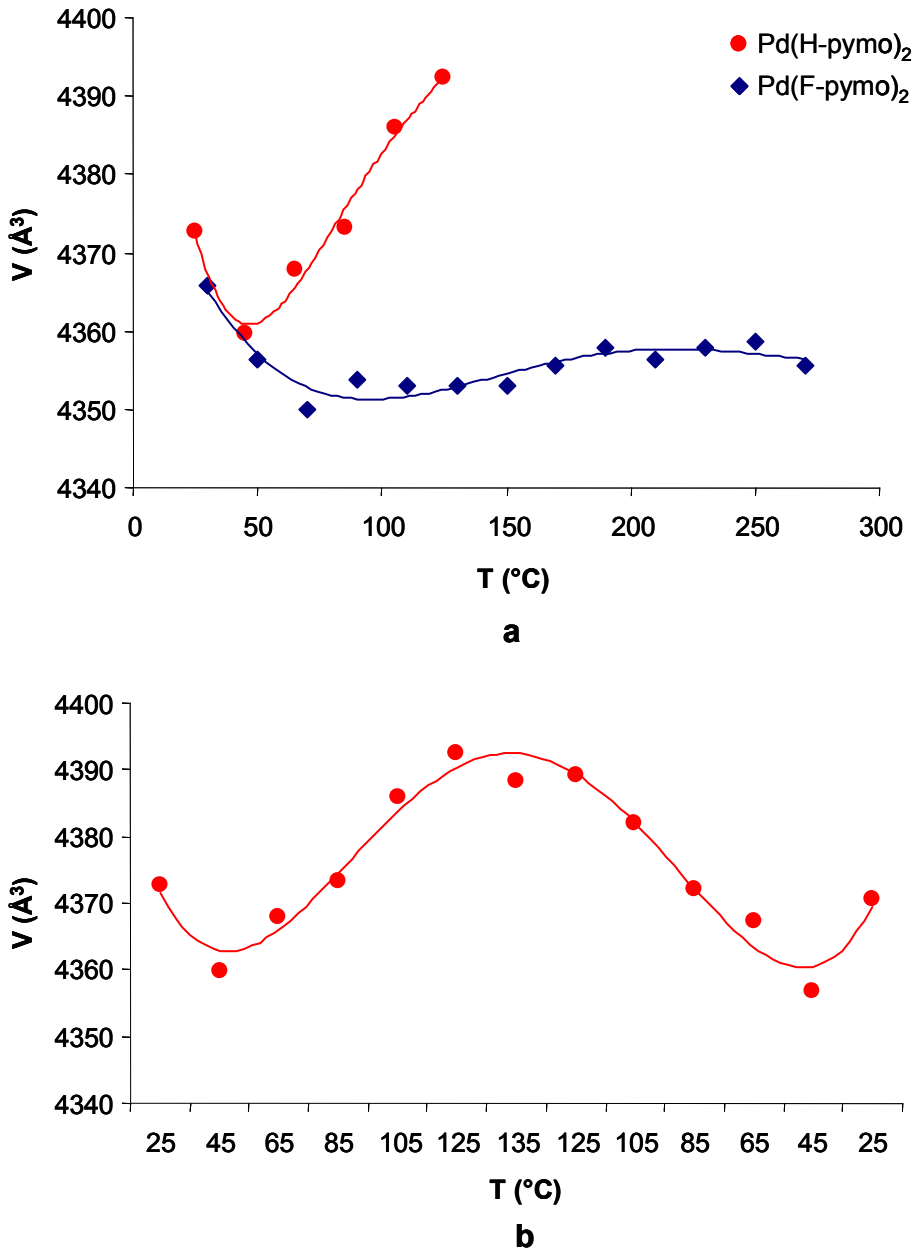

Figure 2. Thermodiffractometric experiments performed on species $\mathbf{2_H}$ (red circles) and $\mathbf{2_F}$ (blue diamonds): a) unit cell volume modification, on raising the temperature, for $\mathbf{2_H}$ and $\mathbf{2_F}$; b) unit cell volume modification for $\mathbf{2_H}$ on performing a whole heating-cooling cycle. The lines have the only scope of guiding the eyes. Note that, despite of the wavy appearance of these curves, the relative maximum changes is well below 1%.

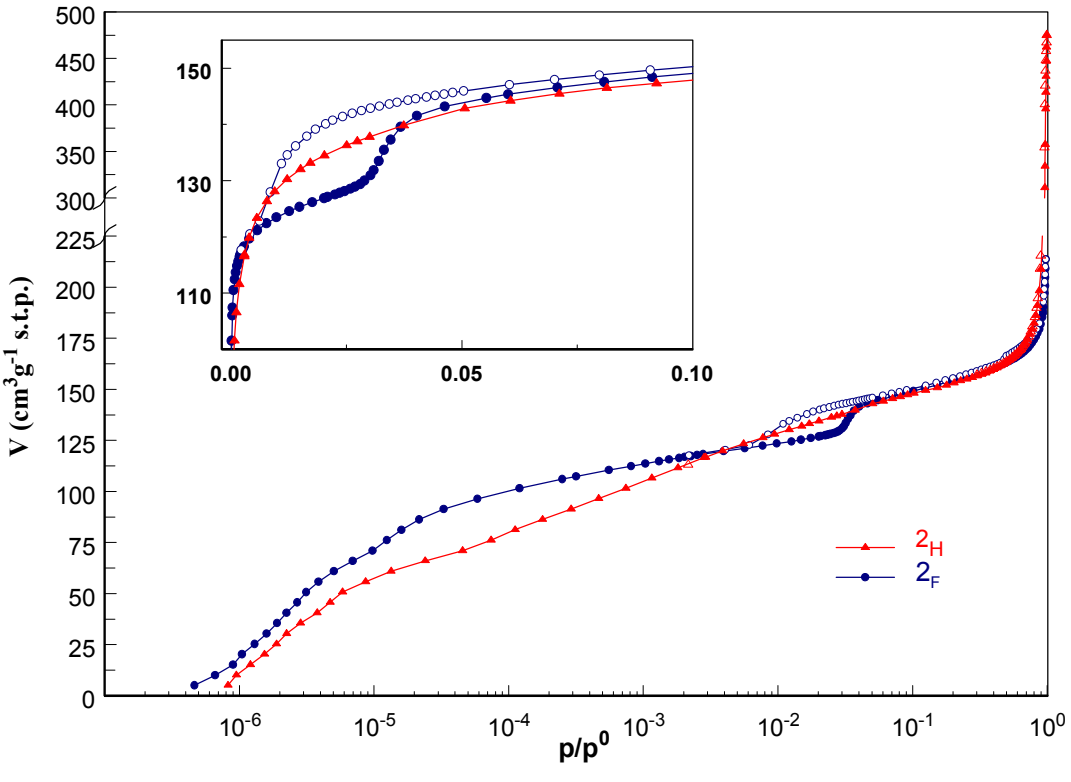

Figure 3. N_2 adsorption isotherms at 77 K for $\mathbf{2_H}$ and $\mathbf{2_F}$. The inset highlight the hysteresis cycle found in the low pressure region of the $\mathbf{2_F}$ isotherm. Desorption is denoted by open symbols.

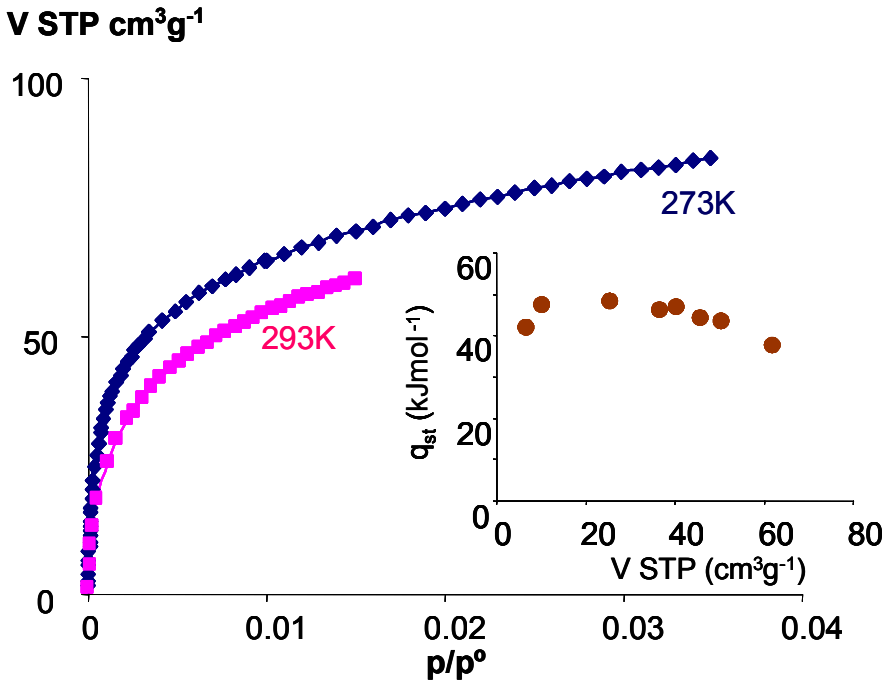

Figure 4. CO_2 adsorption isotherms of $\mathbf{2_F}$ at 273 K (diamonds) and 293 K (squares). Desorption is denoted by open symbols. The inset shows the isosteric heat of adsorption as a function of the amount of sorbed CO_2.

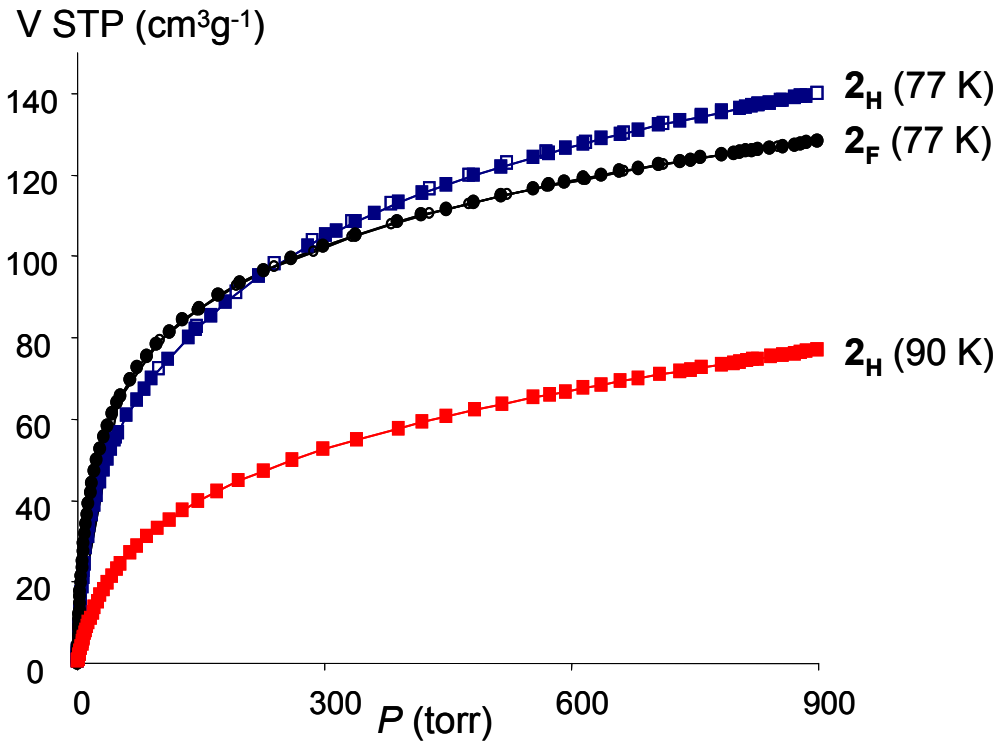

Figure 5. Comparative H_2 adsorption isotherms of $\mathbf{2_H}$ (77 K, black circles, and 90 K, red squares) and $\mathbf{2_F}$ (77 K, blue squares). Desorption is denoted by open symbols.

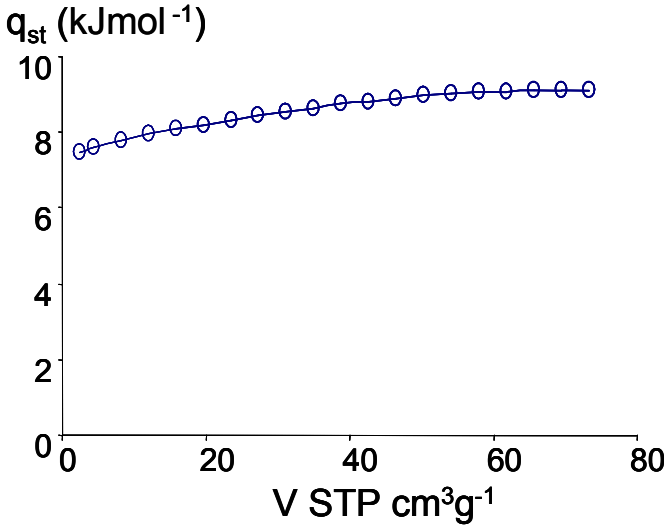

Figure 6. Isosteric heat of adsorption as a function of the amount of sorbed H_2 for $\mathbf{2_H}$.

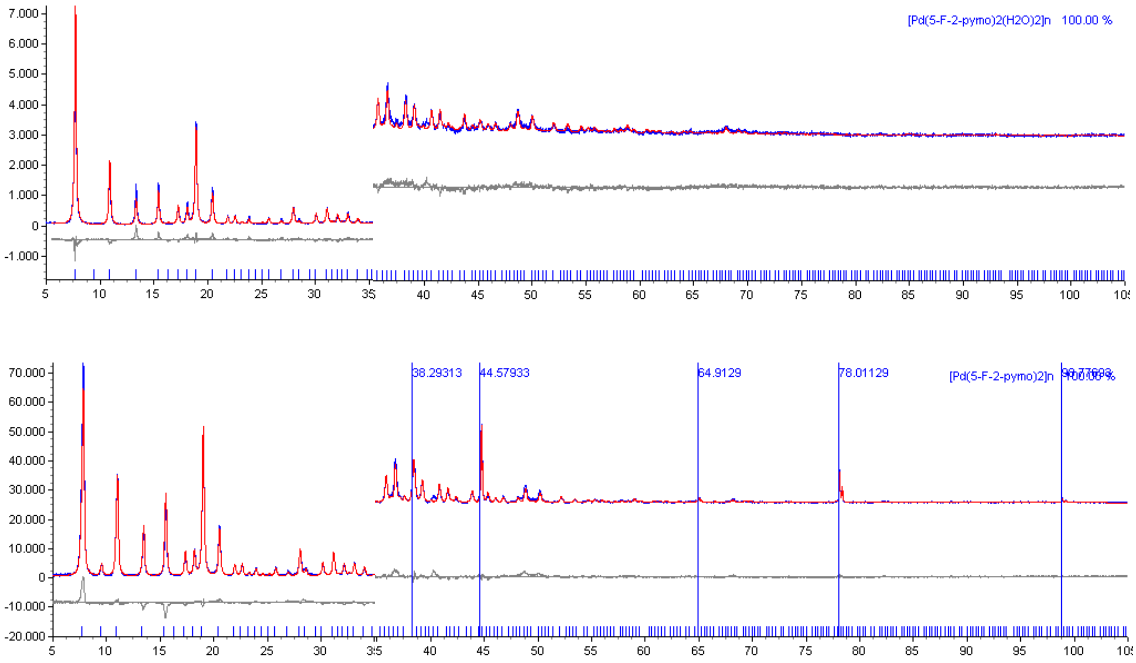

Figure 7. Rietveld refinement results for the hydrated (top) and the anhydrous (bottom) forms of compound $\mathbf{2_F}$ in terms of acquired (blue), calculated (red) and difference (grey) diffractograms, and peak markers. Horizontal axis: 2θ, °; vertical axis: intensity, counts. The portion of the diffractograms above 35° has been magnified for clarity purposes (4×). A few peaks belonging to the aluminium sample-holder are present in the trace of the anhydrous species.

References

1 See *e.g.* (a). M. M. E. Davis, *Nature*, 2002, **417**, 813. (b) L. Schlapbach and A. Züttel, *Nature*, **2001**, *414*, 353. (c) M. Fichtner, *Adv. Eng. Mater*., 2005, **7**, 443.

2 See *e.g.* (a) H. Lee, J. Lee, D. Y. Kim, J. Park, Y. Seo, H. Zeng, I. L. Moudrakovski, C. I. Ratcliffe and J. A. Ripmeester, *Nature*, 2005, **434**, 743. (b) P. Sozzani, S. Bracco, A. Comotti, L. Ferretti and R. Simonutti, *Angew. Chem. Int. Ed*., 2005, **44**, 1816. (c) P. J. Paukstelis, *J. Am. Chem. Soc*., 2006, **128**, 6794.

3 See *e.g.* special issue in *J. Solid. State Chem*. 2005, **178**, 2409-2573.

4 (a) K. Uemura and S. Kitagawa, *Chem. Soc. Rev.*, 2005, **34**, 109. (b) S. Kitagawa, S. Noro and T. Nakamura, *Chem. Commun.*, 2006, 701. (c) J. L. C. Rowsell and O.M. Yaghi, *Microporous Mesoporous Mater*., 2004, **73**, 3.

5 U. Mueller, M. Schubert, F. Teich, H. Puetter, K. Schierle-Arndt and J. Pastre, *J. Mater. Chem*., 2006, **16**, 626.

6 See *e.g.* (a) J. A. Rodríguez Navarro, E. Barea Martínez, J. M. Salas Peregrín, N. Masciocchi, S. Galli, A. Sironi, J. B. Parra Soto and C. Ovín Ania, *PCT/ES 000349, 2006*. (b) U. Mueller, G. Luinstra and O. M. Yaghi, *US Pat*. 6 617 467, 2004, BASF Aktiengesellschaft. (c) R. T Yang, Y. W. Li, G. S. Qi and A. J. Lachawiec, *U.S. Patent application filed*, 2005

7 (a) X. Zhao, B. Xiao, A. J. Fletcher, K. M. Thomas, D. Bradshaw, M. J. Rosseinsky, *Science*, 2004, **306**, 1012. (b) R. Matsuda, R. Kitaura, S. Kitagawa, Y. Kubota, R. V. Belosludov, T. C. Kobayashi, H. Sakamoto, T. Chiba, M. Takata, Y. Kawazoe, Y. Mita, *Nature*, 2005, **436**, 238. (c) S.-i. Noro, R. Kitaura, S. Kitagawa, T. Akutagawa, T. Nakamura, *Inorg. Chem*. 2006, **45**, 8990.

8 T. Uemura, R. Kitaura, Y. Ohta, M. Nagaoka and S. Kitagawa *Angew. Chem. Int. Ed.*, 2006, **45**, 4112.

9 (a) G. Ferey, M. Latroche, C. Serre, F. Millange, T. Loiseau and A. Percheron-Guegon, *Chem. Commun.*, 2003, 2976. (b) B. Chen, N. W. Ockwig, A. R. Millward, D. S. Contreras and O. M. Yaghi, *Angew. Chem. Int. Ed*., 2005, **44**, 4745. (c) X. Lin, J. Jia, X. Zhao, K. M. Thomas, A. J. Blake, G. S. Walker, N. R. Champness, P. Hubberstey, M. Schröder, *Angew. Chem. Int. Ed*., 2006, **45**, 7358.

10 M. Dinca, A. F. Yu and J. R. Long, *J. Am. Chem. Soc*.**,** 2006, **128**, 8904.

11 S. K. Bhatia and A. L. Myers, *Langmuir*, 2006, **22**, 1688.

12 S. Ma and H.-C. Zhou, *J. Am. Chem. Soc***.** 2006, **128**, 11734.

13 (a) L. C. Tabares, J. A. R. Navarro and J. M. Salas, *J. Am. Chem. Soc*., 2001, **123**, 283; (b) E. Barea, J. A. R. Navarro, J. M. Salas, N. Masciocchi, S. Galli and A. Sironi, *Polyhedron*, 2003, **22**, 3051. (c) E. Barea, J. A. R. Navarro, J. M. Salas, N. Masciocchi, S. Galli and A. Sironi, *J. Am. Chem. Soc*., 2004, **125**, 3015. (d) E. Barea, J. A. R. Navarro, J. M. Salas and M. Quirós, *Dalton Trans*., 2005, 1743.

14 J. A. R. Navarro, E. Barea, J. M. Salas, N. Masciocchi, S. Galli, A. Sironi, C. O. Ania and J. B. Parra, *Inorg. Chem.*, 2006, **45**, 2397.

15 N. Masciocchi, S. Galli, A. Sironi, E. Cariati, M. A. Galindo, E. Barea, M. A. Romero, J. M. Salas, J. A. R. Navarro and F. Santoyo-González, *Inorg. Chem.*, 2006, **45**, 7612.

16 M. Fujita, M. Tominaga, A. Hori and B.Therrien, *Acc. Chem. Res*., 2005, **38**, 369.

17 N. Masciocchi, S. Galli and A. Sironi, *Comm. Inorg. Chem.*, 2005, **26**, 1.

18 R. Damgaard Poulsen, A. Bentien, M. Christensen and B. Brummerstedt Iversen, *Acta Cryst.*, 2006, **B62**, 245.

19 Y. Tao, H. Kanoh, L. Abrams, K. Kaneko, *Chem. Rev*. 2006, **106**, 896.

20 R. Kitaura, R. Matsuda, Y. Kubota, S. Kitagawa, M. Takata, T. C. Kobayashi and M. Suzuki, *J. Phys. Chem. B*, 2005, **109**, 23378.

21 M. Dinca, A. F. Yu, J. R. Long, *J. Am. Chem. Soc.* 2006, **128**, 8904.

22 D. Li and K. Kaneko, *J. Phys. Chem. B*, 2000, **104**, 8940.

23 P. Metrangolo, H. Neukirch, T. Pilati, and G. Resnati, *Acc. Chem. Res.*, 2005, **38**, 386.

24 G. Férey, personal communication.

25 S. Bourrelly, P. L. Llewellyn, C. Serre, F. Millange, T. Loiseau and G. Ferey, *J. Am. Chem. Soc.*, 2005, **127**, 13519.

26 J. A. Dunne, M. Rao, S. Sircar, R. J. Gorte, A. L. Myers, *Langmuir*, 1996, **12**, 5896.

27 B. Chen, N. W. Ockwig, A. R. Millward, D. S. Contreras and O. M. Yaghi, *Angew. Chem. Int. Ed*., 2005, **44**, 4745.

28 The relative surface coverage can be calculated by assuming that the monolayer condensation of hydrogen on a solid surface leads to a maximum of 1.3 10^{-5} mol m^{-2} of adsorbed hydrogen.[1b]

29 D. N. Dybtsev, H. Chun, S. H. Yoon, D. Kim and K. Kim, *J. Am. Chem. Soc.*, 2004, **126**, 32.

30 S. S. Kaye and J. R. Long, *J. Am. Chem. Soc*., 2005, **127**, 6506.

31 A. Zecchina, S. Bordiga, J. G. Vitillo, G. Ricchiardi, C. Lamberti, G. Spoto, M. Bjørgen and K. P. Lillerud, *J. Am. Chem. Soc*., 2005, **127**, 6361.

32 S. M. N. Efange, E. M. Alessi, H. C. Shih, Y. C. Cheng and T. J. Bardos, *J. Med. Chem.*, 1985, **28**, 904.

33 Topas-R, Bruker AXS: General profile and structure analysis software for powder diffraction data.

34 A. A. Coelho, *J. Appl. Crystallogr.*, 2000, **33**, 899.

35 R. W. Cheary and A. A. Coelho, *J. Appl. Crystallogr.*, 1992, **25**, 109.